

# 000 001 002 003 004 005 DYSLEXIFY: A MECHANISTIC DEFENSE AGAINST TY- 006 POGRAPHIC ATTACKS IN CLIP 007 008 009

010 **Anonymous authors**  
011 Paper under double-blind review  
012  
013  
014  
015  
016  
017  
018  
019  
020  
021  
022  
023  
024  
025  
026

## ABSTRACT

027 Typographic attacks exploit multi-modal systems by injecting text into images,  
028 leading to targeted misclassifications, malicious content generation and even Vision-  
029 Language Model jailbreaks. In this work, we analyze how CLIP vision encoders  
030 behave under typographic attacks, locating specialized attention heads in the latter  
031 half of the model’s layers that causally extract and transmit typographic informa-  
032 tion to the `cls` token. Building on these insights, we introduce Dyslexify – a  
033 method to defend CLIP models against typographic attacks by selectively ablating  
034 a typographic circuit, consisting of attention heads. Without requiring finetuning,  
035 Dyslexify improves performance by up to 22.06% on a typographic variant of  
036 ImageNet-100, while reducing standard ImageNet-100 accuracy by less than 1%,  
037 and demonstrate its utility in a medical foundation model for skin lesion diagnosis.  
038 Notably, our gradient-free approach remains competitive with current state-of-the-  
039 art typographic defenses that rely on finetuning. To this end, we release a family  
040 of dyslexic CLIP models which are significantly more robust against typographic  
041 attacks. These models serve as suitable drop-in replacements for a broad range of  
042 safety-critical applications, where the risks of text-based manipulation outweigh  
043 the utility of text recognition.  
044

## 1 INTRODUCTION

045 CLIP models are increasingly adopted as general-purpose vision–language representations, enabling  
046 applications in zero-shot classification, retrieval, diffusion-based generative models, and large-scale  
047 vision–language models (VLMs). Their versatility has further driven adoption in safety-relevant  
048 domains such as healthcare (Yang et al., 2024; Wang et al., 2022; Eslami et al., 2023), remote sensing  
049 (Liu et al., 2024a; Vivanco et al., 2023; Li et al., 2023), and content moderation (Schuhmann et al.,  
050 2022; Liu et al., 2025; Reyes et al., 2025). However, despite their widespread use, CLIP models  
051 remain vulnerable to typographic attacks: inserting text into an image can mislead classification,  
052 trigger malicious generations, or even jailbreak multi-modal systems (see Fig. 1).  
053

054 Existing defenses against typographic attacks require gradient-based optimization. While effective to  
055 some extent, these methods require substantial computational resources and lack interpretability into  
056 the mechanisms underlying CLIP’s behavior.  
057

058 In this work, we introduce Dyslexify a gradient-free defense that directly targets model circuits  
059 responsible for the vulnerability to typographic attacks. By identifying and ablating a set of attention  
060 heads with demonstrable causal effects, we construct dyslexic CLIP models that are substantially  
061 more robust to typographic attacks. Our method scales seamlessly to billion-parameter models,  
062 making it applicable to state-of-the-art multi-modal systems. Beyond improving robustness, our  
063 approach also enhances interpretability of CLIP models, enabling targeted intervention that are  
064 computationally efficient and easily integrated into existing pipelines without additional overhead.  
065

066 The contributions of this work are:  
067

- 068 • **Mechanistic Understanding:** We present the Typographic Attention Score to locate spe-  
069 cialized typographic attention heads and demonstrate their causal role in typographic attacks  
070 within CLIP models through controlled interventions.  
071
- 072 • **Gradient-Free Defense:** We introduce a method that utilizes circuit ablation to effectively  
073 defend against typographic attacks, while maintaining general visual capabilities. Due to its  
074

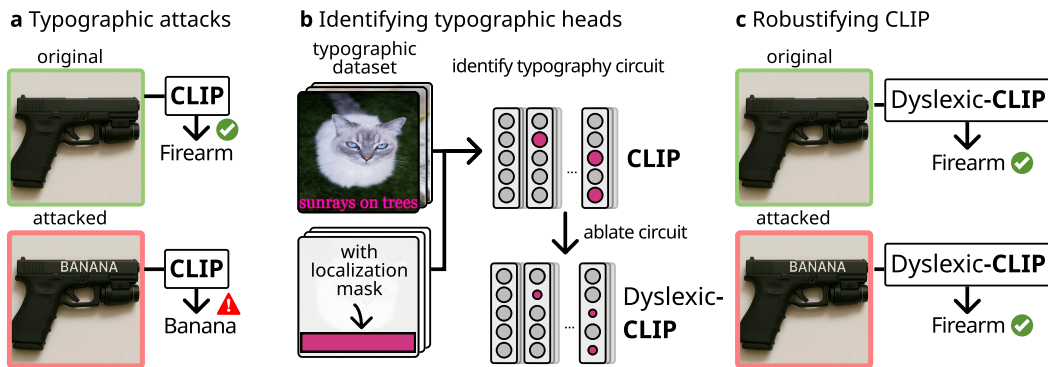


Figure 1: Defending CLIP against typographic attacks with Dyslexify a) Adversarial text in images can dominate CLIP’s representation and lead to misclassification. b) We construct a circuit of attention heads responsible for transmitting typographic information. c) By suppresses the typographic circuit, we defend against typographic attacks without a single gradient step.

gradient-free nature, Dyslexify seamlessly scales to billion-parameter models on consumer grade hardware.

- **Empirical Validation:** We validate Dyslexify across a diverse set of zero-shot classification tasks, demonstrating that our approach improves robustness to typographic attacks by up to 22.06% on a typographic version of Imagenet-100 while maintaining high accuracy on non-typographic benchmarks.
- **Medical Use Case:** We show that typographic attacks pose a tangible risk to safety-critical medical foundation models, and demonstrate that Dyslexify can substantially mitigate this vulnerability.
- **Model Release:** To facilitate safer deployment, we release a family of dislexic CLIP models with reduced typographic sensitivity, suitable for use in safety-critical applications.

Our approach provides a practical, interpretable, and computationally efficient typographic defense, paving the way for safer multimodal systems without the need for fine-tuning. Code is available at <https://anonymous.4open.science/r/Dyslexify-4BA8>.

## 2 RELATED WORK

CLIP models (Radford et al., 2021) are pretrained on large-scale image–text datasets such as Laion-5b (Schuhmann et al., 2022), aligning global image features with textual descriptions for strong zero-shot transfer. This reliance on textual supervision also makes them vulnerable to typographic attacks.

Typographic attacks (Goh et al., 2021) insert written text into an image to maliciously alter a model’s behavior. Recent work demonstrates that typographic attacks can degrade model performance, bypass safety filters (jailbreaking) and hijack goals in Vision Language Models (VLMs) (Qraitem et al., 2024; Kimura et al., 2024; Gong et al., 2025; Cao et al., 2024; Westerhoff et al., 2025), trigger harmful content generation in image-to-image pipelines (Cheng et al., 2024), and cause targeted misclassification in object detection and zero-shot classification settings (Materzyńska et al., 2022; Ilharco et al., 2022; Azuma & Matsui, 2023; Westerhoff et al., 2025; Dreyer et al., 2025).

Several defenses have been proposed, they rely either on fine-tuning the model (Ilharco et al., 2022), learning a projection matrix (Materzyńska et al., 2022), incorporating a learnable text-token called Defense-Prefix (Azuma & Matsui, 2023), or employing Sparse Autoencoders (Joseph et al., 2025). Crucially, none of these approaches offer a gradient-free method for mitigating typographic attacks. In contrast, our work introduces a controllable intervention at inference time by directly locating and suppressing the components responsible for typographic sensitivity, without requiring gradients or fine-tuning.

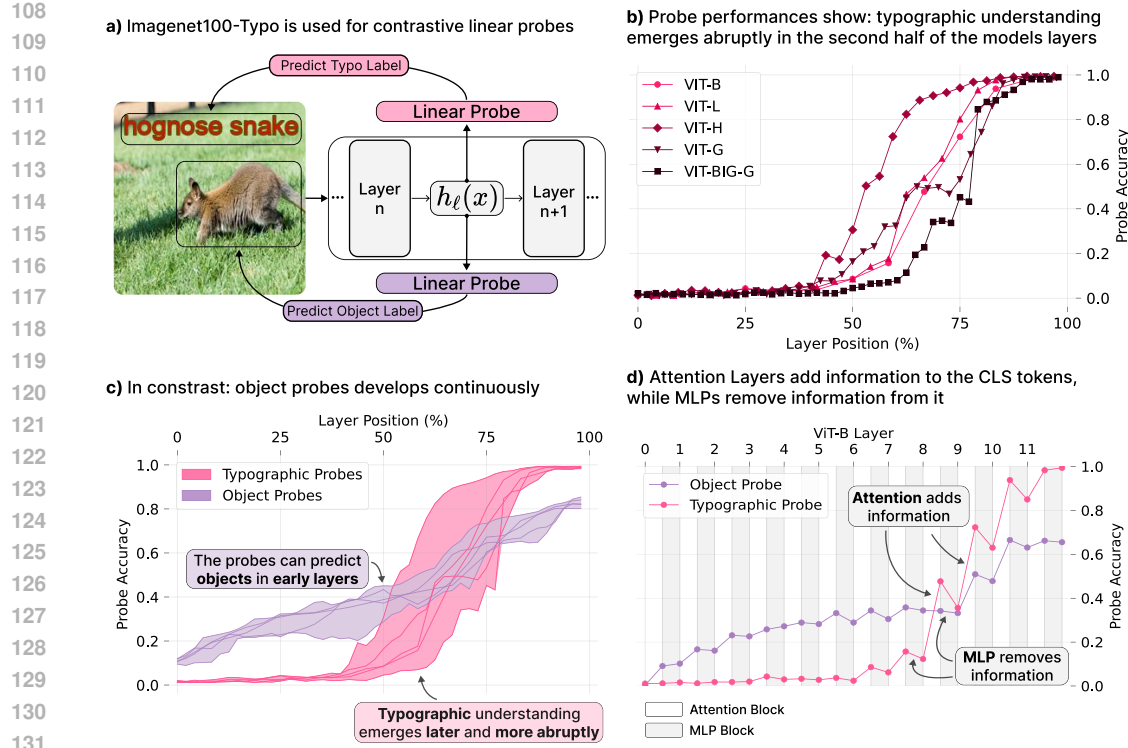


Figure 2: Investigating where typographic understanding emerges in CLIP. **a)** We train two linear probes on all layers of CLIP models. Probe  $P_{\text{img},\ell}$  is used to predict the text label of each sample while  $P_{\text{typo},\ell}$  is trained to predict the typographic class. **b)**  $P_{\text{typo},\ell}$  shows a consistent pattern across all model sizes: typographic information emerges abruptly in the second half of the models layers. **c)** This trend is not true for the object probes  $P_{\text{img},\ell}$ . Object specific information builds gradually over the layers. Each line in the shaded area represents one CLIP model. **d)** While attention layers seem to add linearly decodable information to the `cls` token, MLP layers remove or obscure information.

### 3 MOTIVATION: LOCATING LAYERS OF TYPOGRAPHIC UNDERSTANDING

To better understand CLIP’s vulnerability to typographic attacks and to motivate our method, we begin by investigating which layers and components are responsible for typographic understanding using linear probes.

**Typographic datasets:** We further construct typographic attack datasets from standard image classification datasets  $D = \{(x_i, y_i)\}_{i=1}^n$  by assigning each input example  $x_i$  an additional typographic label  $z_i \neq y_i$  different from the original label  $y_i$ , and overlaying a corresponding textual description of  $z_i$  onto the original image  $x_i$  at a random location as shown in Fig. 2a. We denote these modified datasets with the suffix “-typo”. More information on the datasets is provided Appendix F.

Extending the ImageNet-100 dataset into the ImageNet-100-typo dataset, we can evaluate typographic understanding by training linear probes on the `cls` token embedding at each layer of OpenCLIP models, ranging in scale from ViT-B to ViT-bigG (Ilharco et al., 2021).

Formally, for a layer  $\ell$  we define a linear probe  $P_\ell$

$$\hat{y}_\ell(x) = w^\top h_{\text{cls}}^\ell + b, \quad (1)$$

where  $h_{\text{cls}}^\ell \in \mathbb{R}^d$  denotes the activation of the model at layer  $\ell$  on the `cls` token for an input sample  $x$ , and  $w$  and  $b$  are the probe’s weight vector and bias term, respectively. We train two types of probes:  $P_{\text{img},\ell}$ , which predicts the object label  $y$  and  $P_{\text{typo},\ell}$ , which predicts the typographic label  $z$ . The accuracy of a probe  $P$  is denoted by  $\text{Acc}(P)$ .

162 Fig. 2b shows that  $\text{Acc}(P_{\text{typo},\ell}) > 0.99$  at the final layer for all tested models, indicating that CLIP  
 163 models can distinguish the typographic classes. Furthermore it shows, that  $\text{Acc}(P_{\text{typo},\ell})$  is low in  
 164 early layers, but exhibit a sharp increase in the latter half of the model.

165 Fig. 2c shows that  $\text{Acc}(P_{\text{img},\ell})$  improves gradually over the layers, while  $\text{Acc}(P_{\text{typo},\ell})$  exhibits a sharp  
 166 performance rise around second half of the models layers.

167 Fig. 2d highlights the effect of the attention and the MLP blocks onto  $\text{Acc}(P_{\text{img},\ell})$  and  $\text{Acc}(P_{\text{typo},\ell})$ .  
 168 Attention layers consistently improve accuracy indicating that they add linearly decodable information  
 169 to the `cls` token. In contrast, the MLP layers tend to reduce accuracy. We show in Appendix B, that  
 170 the Intrinsic Dimensionality (ID) of the signal decreases after the MLP blocks, suggesting that the  
 171 MLP compresses or discards information.

## 173 4 DYSLEXIFY: A DEFENSE AGAINST TYPOGRAPHIC ATTACKS

174 To defend CLIP against typographic attacks we present Dyslexify: a framework for detecting and  
 175 suppressing typographic circuits. Based on the finding in Section 3 that attention heads are responsible  
 176 for adding typographic information, we only consider attention heads for the circuit construction. We  
 177 define a circuit as a subset  $\mathcal{C} \subseteq \Psi$ , where  $\Psi$  denotes the set of attention heads in CLIP

$$178 \Psi = \{\mathcal{H}_{i,\ell} \mid i \in \{0, \dots, I\}, \ell \in \{0, \dots, L\}\} \quad (2)$$

179 with  $I$  heads per layer and  $L$  layers in total, where  $\mathcal{H}_{i,\ell}$  denote the  $i$ th attention head in layer  $\ell$ .

180 To robustify a model  $\mathcal{M}$  against typographic attacks, we conduct *circuit-ablation* of a typographic  
 181 circuit  $\mathcal{C}$ . Circuit-ablation modifies here only the residual stream of the `cls` token, leaving all other  
 182 computations intact. Specifically, the residual update of the `cls` token is given by

$$183 z_{\text{cls}}^\ell = h_{\text{cls}}^\ell + \text{MLP}(h_{\text{cls}}^\ell) \quad (3)$$

$$184 h_{\text{cls}}^{\ell+1} = z_{\text{cls}}^\ell + \sum_{i=1}^H \mathcal{H}_{i,\ell,\text{cls}}(z_{\text{cls}}^\ell) \quad (4)$$

185 where  $z_{\text{cls}}^\ell$  is the `cls` activation after the layer- $\ell$  MLP block is applied to  $h_{\text{cls}}^\ell$ , and  $\mathcal{H}_{i,\ell,\text{cls}}(z_{\text{cls}}^\ell)$  is the  
 186 contribution of head  $\mathcal{H}_{i,\ell}$  to the `cls` token.

187 We define ablation of a typographic circuit  $\mathcal{C}$  as

$$188 \mathcal{H}_{i,\ell,\text{cls}}(z_{\text{cls}}^\ell) \leftarrow 0 \quad \text{for all } \mathcal{H}_{i,\ell} \in \mathcal{C}, \quad (5)$$

189 while leaving all spatial contributions unchanged. We use  $\mathcal{M}_{\mathcal{C}}$  to denote a model  $\mathcal{M}$  in which circuit  
 190  $\mathcal{C}$  is ablated.

### 191 4.1 TYPOGRAPHIC ATTENTION SCORE

192 Building on Hung et al. (2024) we introduce the Typographic Attention Score  $T_{i,\ell}$  to guide the circuit  
 193 construction. Intuitively the score measures the amount of spatial attention a head  $\mathcal{H}_{i,\ell}$  dedicates to  
 194 typographic content.

195 Given a head  $\mathcal{H}_{i,\ell}$  and an input  $x$ , we write  $A_{i,\ell}(x) \in [0, 1]^{T+1}$  to denote the `cls` tokens attention  
 196 pattern, where  $T$  is the number of spatial tokens and the additional entry corresponds to the `cls`  
 197 token. We further define the spatial `cls`-attention pattern  $A_{i,\ell}^*(x) \in [0, 1]^T$  which excludes the  
 198 `cls-to-cls` entry  $A_{i,\ell,\text{cls}}(x)$ , such that

$$199 A_{i,\ell}(x) = (A_{i,\ell,\text{cls}}(x), A_{i,\ell}^*(x)). \quad (6)$$

200 We write  $A_{i,\ell,t}^*(x)$  to index the  $t$ th element of the pattern. Formally the score is given by:

$$201 T_{i,\ell} = \sum_{x \in \mathcal{D}} \frac{\sum_{t=1}^T \mathbb{1}(t) A_{i,\ell,t}^*(x)}{\sum_{t=1}^T A_{i,\ell,t}^*(x)}. \quad (7)$$

202 Where  $x$  is a data point,  $\mathcal{D}$  is the dataset, and  $\mathbb{1}$  is an indicator function so that  $\mathbb{1}(t) = 1$  if the input  
 203 patch associated with the token at index  $t$  corresponds to typographic content and is zero otherwise.

216 4.2 TYPOGRAPHIC CIRCUIT CONSTRUCTION  
217

218 To defend against typographic attacks without degrading zero-shot classification, Dyslexify constructs  
219 a typographic circuit  $\mathcal{C}$ . The circuit is built iteratively while monitoring the accuracy of the circuit-  
220 ablated model  $\mathcal{M}_C$  on a non-typographic benchmark  $D_{\text{img}}$  and a typographic benchmark  $D_{\text{typo}}$ ,  
221 ensuring that the accuracy on  $D_{\text{img}}$  never decreases by more than a threshold  $\epsilon \in \mathbb{R}$ .

222 Our procedure consists of two steps: (i) rank all attention heads  $\mathcal{H}_{i,\ell}$  by their typographic score  $T_{i,\ell}$ ;  
223 (ii) add heads to  $\mathcal{C}$  in descending order of  $T_{i,\ell}$ , evaluating accuracy after each addition.

224 Let  $\text{Acc}(\mathcal{M}, D)$  denote the accuracy of model  $\mathcal{M}$  on dataset  $D$ . For each candidate head  $\mathcal{H}$ , we  
225 compute  
226

$$\Delta\text{Acc}_{\text{img}} = \text{Acc}(\mathcal{M}, D_{\text{img}}) - \text{Acc}(\mathcal{M}_{\mathcal{C} \cup \mathcal{H}}, D_{\text{img}}), \quad (8)$$

$$\Delta\text{Acc}_{\text{typo}} = \text{Acc}(\mathcal{M}_{\mathcal{C} \cup \mathcal{H}}, D_{\text{typo}}) - \text{Acc}(\mathcal{M}_C, D_{\text{typo}}), \quad (9)$$

230 where  $\Delta\text{Acc}_{\text{img}}$  measures the accuracy drop on  $D_{\text{img}}$  relative to the base model, and  $\Delta\text{Acc}_{\text{typo}}$   
231 measures the incremental gain on  $D_{\text{typo}}$  from adding head  $\mathcal{H}$  to the current circuit  $\mathcal{C}$ .

232 If  $\Delta\text{Acc}_{\text{typo}} \leq 0$ , the head  $\mathcal{H}$  is skipped, as it does not improve robustness to typographic attacks. If  
233 the head is not skipped and  $\Delta\text{Acc}_{\text{img}} < \epsilon$ , the head is added to  $\mathcal{C}$ ; otherwise, the algorithm terminates.  
234 In addition, if more than  $k \in \mathbb{N}$  heads are skipped consecutively, the algorithm also terminates.

235 We refer to the final model  $\mathcal{M}_C$ , equipped with the constructed circuit  $\mathcal{C}$ , as the *dyslexic model*.

237 **Algorithm 1** Dyslexify  
238

```

239 1: Initialize circuit  $\mathcal{C} \leftarrow \emptyset$ , skip counter  $s \leftarrow 0$ .
240 2: Set hyperparameters: tolerance  $\epsilon$ , max skips  $k$ .
241 3: Rank heads  $\mathcal{H}_{i,\ell}$  by score  $T_{i,\ell}$ .
242 4: for head  $\mathcal{H}_{i,\ell}$  in descending order of  $T_{i,\ell}$  do
243 5:   Compute  $\Delta\text{Acc}_{\text{img}}$ ,  $\Delta\text{Acc}_{\text{typo}}$ .
244 6:   if  $\Delta\text{Acc}_{\text{typo}} \leq 0$  then
245 7:      $s \leftarrow s + 1$ ;
246 8:     if  $s \geq k$  then break; end if
247 9:     continue;
248 10:   end if
249 11:   if  $\Delta\text{Acc}_{\text{img}} \geq \epsilon$  then break; end if
250 12:   Add  $\mathcal{H}_{i,\ell}$  to  $\mathcal{C}$ ;  $s \leftarrow 0$ .
251 13: end for
252 14: Return final circuit  $\mathcal{C}$ .
```

253 5 EXPERIMENTS  
254

## 255 5.1 EVALUATING THE TYPOGRAPHIC ATTENTION SCORE

256 We construct localized typographic dataset consisting of 10,000 natural images from Unsplash<sup>1</sup>,  
257 originally containing minimal typographic content. To efficiently analyze the attention patterns, we  
258 synthetically introduce typographic content at the bottom center of the image, responding to the  
259 lowest two token rows in the spatial grid.

260 For each attention head  $\mathcal{H}_{i,\ell}$  we extract the attention pattern  $A_{i,\ell}^*(x)$  over this localized dataset. We  
261 use the known spatial bias to define the indicator mask  $\mathbb{1}(t) \in \{0, 1\}$ , where  $\mathbb{1}(t) = 1$  at the the  
262 typographic region and  $\mathbb{1}(t) = 0$  elsewhere.

263 Fig. 3 shows the resulting Typographic Attention Scores  $T_{i,\ell}$  for ViT-B. A small subset of heads  
264 shows high scores of up to  $T_{i,\ell} \geq \mu(T) + 2\sigma(T)$ , revealing a strong spatial bias towards typography.  
265 Furthermore we observe, that the spike in  $\text{Acc}(P_{\text{typo},\ell})$  only occurs after layers with high  $T_{i,\ell}$  heads.  
266 More results can be found in Appendix K.

267

<sup>1</sup><https://huggingface.co/datasets/wtcherr/unsplash>

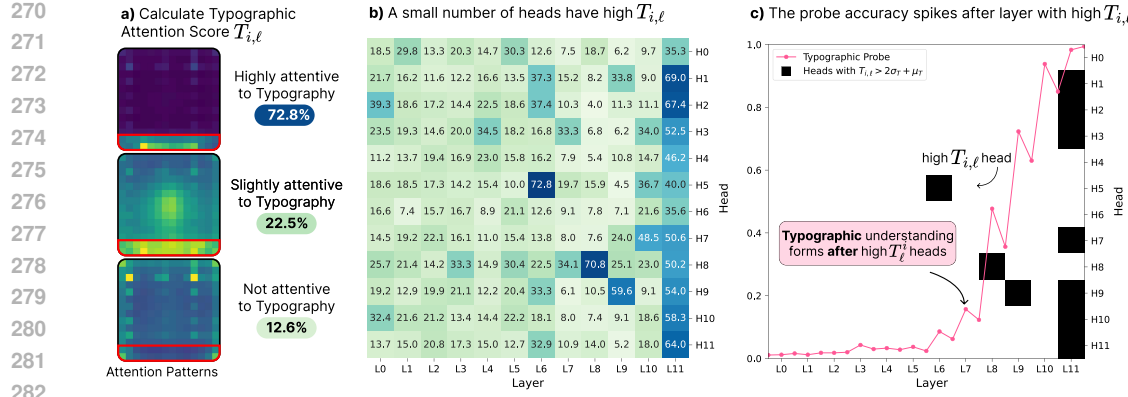


Figure 3: Analysis of the Typographic Attention Score. **a)** For each head in the model we calculate the Typographic Attention Score  $T_{i,\ell}$ , utilizing the spatial bias in the Unsplash-typo dataset. **b)** Depiction of ViT-B’s  $T_{i,\ell}$  scores. While most attention heads do not show any spatial bias in their attention patterns, a few attention heads indicate significantly elevated scores, exceeding  $T_{i,\ell} \geq \mu(T) + 2\sigma(T)$ . Those heads only occur in the second half of the models layers **c)** Overlaying the linear probes with significantly elevated  $T_{i,\ell}$  scores , highlights an interesting correlation. Only after the attention heads with exceptionally high  $T_{i,\ell}$  scores are passed the model the accuracy of  $P_{\text{typo},\ell}$  begins to increase rapidly.

## 5.2 EVALUATING THE TYPOGRAPHIC CIRCUITS

To construct the circuits  $\mathcal{C}$ , we set the tolerance to  $\epsilon = 0.01$ , set the maximum number of consecutive skips to  $k = 10$ , use the ImageNet-100 training split as  $D_{\text{img}}$ , and ImageNet-100-typo as  $D_{\text{typo}}$ . Table 5 shows that the resulting circuits are sparse, covering at most 10.1% of  $\Psi$ .

Fig. 4 plots  $\text{Acc}(\mathcal{M}_C, D_{\text{img}})$  and  $\text{Acc}(\mathcal{M}_C, D_{\text{typo}})$  as heads are added. Dyslexify, improves accuracy on ImageNet-100-typo’s train set by more than 20% across all evaluated models, while limiting the drop in ImageNet-100 accuracy to below 1%. More results can be found in Fig. 9.

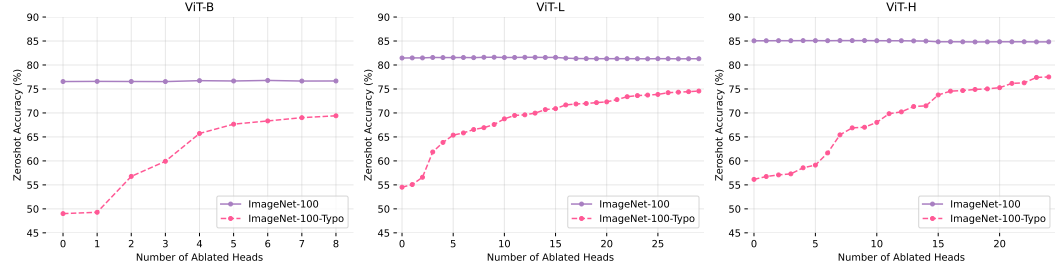


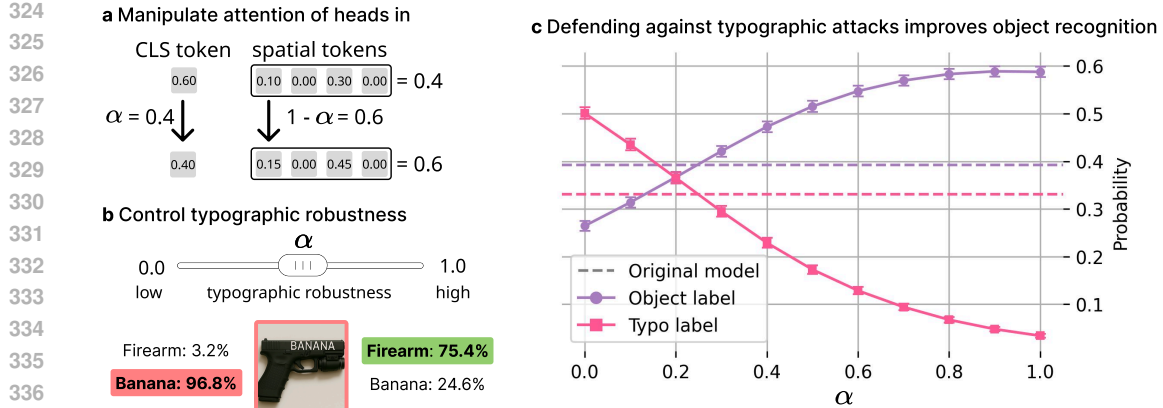
Figure 4: Tradeoff between general accuracy and typographic robustness as a function of the number of ablated heads. Ablations are applied in decreasing order of  $T_{i,\ell}$ .

### 5.2.1 DEMONSTRATING CAUSALITY OF TYPOGRAPHIC CIRCUITS

We observe that attention heads in  $\mathcal{C}$  utilize their `cls` self-attention as attention sinks (Xiao et al., 2023) depending on the presence of typography in the image. Further details are provided in Appendix C. Building on those findings we showcase the causal nature of these attention heads in this section.

To demonstrate the causal role of these heads in typographic vulnerability, we manipulate their attention patterns. Specifically, we construct

$$A_{i,\ell}^\alpha = [\alpha, A_{i,\ell}^* \cdot (1 - \alpha) / \|A_{i,\ell}^*\|], \quad (10)$$



339 Figure 5: Controlling typographic vulnerability by manipulating attention sinks in circuit heads. a)  
340 We set the `cls` token attention to  $\alpha$  and rescale the spatial token attentions to sum to  $1 - \alpha$ . b)  
341 Increasing  $\alpha$  raises attention to spatial tokens, amplifying typographic understanding. c) Decreasing  
342  $\alpha$  increases typographic robustness, increasing the probability of predicting the true object class.

343  
344 where  $\alpha \in \{0.0, 0.1, \dots, 0.9, 1.0\}$ . The scaling factor  $(1 - \alpha)/\|A_{i,\ell}^*\|$  ensures that the attention  
345 distribution remains normalized.

346 We then evaluate the effectiveness of typographic attacks under these manipulations by tracing the  
347 predicted label probabilities  $p(y_{\text{text}})$  and  $p(y_{\text{typo}})$  as a function of  $\alpha$  on the ImageNet-100-typo dataset.  
348

349 **Results:** Fig. 5 shows that increasing  $\alpha$  causally reduces the effectiveness of typographic attacks,  
350 while decreasing  $\alpha$  amplifies it. This provides direct causal evidence: as circuit heads allocate more  
351 weight to the `cls` sink, the attack signal is suppressed; conversely, when  $\alpha$  is low and spatial attention  
352 dominates,  $p(y_{\text{typo}})$  increases, indicating that typographic information is transferred from spatial  
353 tokens into the `cls` representation.

### 356 5.3 EVALUATING THE DISLEXIC MODELS

357 To evaluate Dyslexify we construct dyslexic OpenClip model variants: ViT-B, L, H, G, and BigG  
358 and conduct zero-shot classification experiments. Concretely we first evaluate the effectiveness of  
359 our defense against typographic attacks and secondly measure the zero-shot object classification  
360 capabilities on non-typographic datasets. For each model, we record the accuracy difference between  
361 the original model and dyslexic model. A detailed description of the datasets is given in Appendix F.  
362

363 **Results:** Table 1 shows that Dyslexify yields consistent robustness improvements across both real-  
364 world typographic attack datasets and synthetic benchmarks. The observed gains are substantial – up  
365 to +31% accuracy – and occur across all evaluated datasets, suggesting that the identified typographic  
366 circuits capture generalizable failure modes rather than dataset-specific artifacts.

367 Table 2 further demonstrates that Dyslexify preserves performance on standard vision datasets. In  
368 nearly all cases, deviations remain within  $\pm 1\%$  of the base model, the only exception being ViT-L  
369 showing the largest decline ( $-1.74\%$ ) on Aircraft and ( $-1.17\%$ ) on Food-101, which is close to the  
370 tolerance bound  $\epsilon = 1\%$ . This indicates that Dyslexify achieves a favorable robustness–accuracy  
371 trade-off: substantial robustness gains are obtained while standard zero-shot performance is essentially  
372 maintained.

### 374 5.4 COMPARING TO BASELINES

375 We compare Dyslexify to Defense-Prefix (DP) (Azuma & Matsui, 2023), which introduces a learnable  
376 prefix token for CLIP’s language transformer on OpenCLIP ViT-L without fine-tuning the full ViT.

378  
 379 Table 1: Comparison of dyslexic model performance on datasets of typographic attacks across model  
 380 sizes, showing accuracy changes relative to the base model, with improvements ( $\uparrow$ ) or declines ( $\downarrow$ ). IN  
 381 denotes ImageNet, and the suffix -T indicates the corresponding typographic version of the dataset.

382 383 Model	384 Real Typographic			385 Synthetic Typographic		
	386 RTA-100	387 Disentangling	388 Paint	389 IN-100-T	390 Food-101-T	391 Aircraft-T
B	68.30 $\uparrow$ 12.00	85.00 $\uparrow$ 31.11	72.73 $\uparrow$ 14.55	66.84 $\uparrow$ 19.90	78.27 $\uparrow$ 22.64	16.23 $\uparrow$ 5.91
L	71.00 $\uparrow$ 16.60	60.56 $\uparrow$ 10.00	76.36 $\uparrow$ 14.55	72.22 $\uparrow$ 20.32	82.15 $\uparrow$ 26.55	23.34 $\uparrow$ 9.51
H	68.30 $\uparrow$ 15.20	72.22 $\uparrow$ 26.67	70.91 $\uparrow$ 21.82	75.34 $\uparrow$ 21.26	83.01 $\uparrow$ 28.68	29.40 $\uparrow$ 8.07
G	62.00 $\uparrow$ 12.00	67.22 $\uparrow$ 9.44	71.82 $\uparrow$ 16.36	68.76 $\uparrow$ 22.06	73.05 $\uparrow$ 20.21	27.69 $\uparrow$ 3.45
Big-G	72.90 $\uparrow$ 11.90	68.33 $\uparrow$ 20.00	69.09 $\uparrow$ 21.82	78.64 $\uparrow$ 16.74	84.69 $\uparrow$ 25.98	41.61 $\uparrow$ 16.29

392 Table 2: Comparison of dyslexic model performance on non-typographic datasets across model sizes,  
 393 showing accuracy changes relative to the base model, with improvements ( $\uparrow$ ) or declines ( $\downarrow$ ).

394 Model	395 Not Typographic		
	396 Aircraft	397 Food-101	398 ImageNet-100
B	27.72 $\downarrow$ 0.12	84.97 $\downarrow$ 0.99	75.00 $\uparrow$ 0.64
L	34.62 $\downarrow$ 1.74	89.31 $\downarrow$ 1.17	79.52 $\downarrow$ 0.24
H	43.98 $\uparrow$ 0.12	92.29 $\downarrow$ 0.24	83.40 $\downarrow$ 0.34
G	44.07 $\downarrow$ 0.30	91.47 $\downarrow$ 0.70	82.58 $\downarrow$ 0.66
Big-G	50.47 $\downarrow$ 0.39	92.55 $\downarrow$ 0.42	84.72 $\downarrow$ 0.34

401  
 402 Following their setup, we train the DP on the ImageNet-100-typo training split with a learning rate of  
 403 0.002, batch size of 64, and hyperparameters  $\gamma = 3.0$  and  $\eta = 1.0$  for 6 epochs.

404  
 405 Table 3 shows that Dyslexify outperforms DP on two out of three typographic benchmarks, while  
 406 DP retains slightly higher performance on two out of three non-typographic benchmarks. Notably,  
 407 DP yields a modest accuracy improvement on the corresponding non-typographic ImageNet-100,  
 408 likely caused by the choice of ImageNet-100-typo as the training set for DP. We hypothesize that  
 409 the black-box optimization in DP captures features relevant not only to typographic defense but  
 410 also to ImageNet-100 classification, thereby limiting its generalization. In contrast, our method  
 411 focuses on key mechanisms relevant to typographic attacks, leading to more robust transfer across  
 412 non-typographic benchmarks.

413  
 414 Table 3: Performance comparison of Dyslexify and Defense-Prefix (DP) on ViT-L across typographic  
 415 and non-typographic datasets. For each method we show the accuracy followed by the deviation from  
 416 the baseline, ( $\uparrow$ ) for improvement, ( $\downarrow$ ) for decline.

417 418 Method	419 Real Typographic			420 Training		421 Non-Typographic	
	422 RTA-100	423 Disentangling	424 PAINT	425 ImageNet-100	426 Food-101	427 Aircraft	428
Baseline	54.40	50.56	61.81	79.76	90.48	36.36	429
DP	62.20 $\uparrow$ 7.80	82.78 $\uparrow$ 32.20	71.82 $\uparrow$ 10.01	81.70 $\uparrow$ 1.94	89.83 $\downarrow$ 0.65	32.94 $\downarrow$ 3.42	430
Dyslexify	71.00 $\uparrow$ 16.60	60.56 $\uparrow$ 10.00	76.36 $\uparrow$ 14.55	79.52 $\downarrow$ 0.24	89.31 $\downarrow$ 1.17	34.62 $\downarrow$ 1.74	431

## 424 5.5 DEFENDING AGAINST TYPOGRAPHIC ATTACKS IN MELANOMA DETECTION

425 Safety-critical domains such as medicine are particularly vulnerable, as AI decisions may impact  
 426 human lives. Therefore, we investigate whether typographic attacks transfer to this setting and  
 427 whether our defense remains effective. Specifically, we analyze WhyLesionCLIP, a foundation model  
 428 for skin lesion classification (Yang et al., 2024), i.e., melanoma detection, based on OpenClip-ViT-L.

429 We utilize the same setting as in Section 5.1 retrieving the typographic attention scores, but deviate  
 430 from Section 5.2 in that we construct  $\mathcal{C}$  by setting ISIC2019 as  $D_{\text{img}}$  and ISIC2019-Typo as  $D_{\text{typo}}$ .

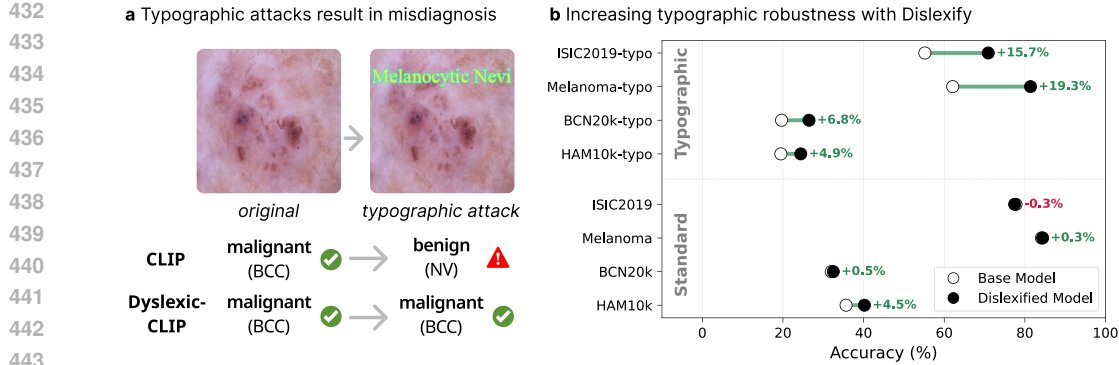


Figure 6: Typographic attacks in melanoma detection. (a) Adding adversarial text may cause CLIP to misdiagnose a malignant lesion as benign. (b) Applying Dyslexify mitigates these failures, increasing robustness to typographic attacks and even improving accuracy in several non-attacked cases.

The results in Fig. 6 and in Table 4 reveal two key insights: (i) Typographic attacks reduce the zero-shot accuracy of melanoma detection by up to 22% and (ii) Dyslexify proves effective in defending a medical foundation model from a relevant attack vector. Not only does Dyslexify increase the accuracy under typographic attack by up to 19.3%, but it also increases the base models accuracy in three out of the four datasets. An additional medical use-case is analyzed in Appendix E.

## 6 CONCLUSION

We present a mechanistic defense against typographic attack in CLIP using an interpretability-first approach. We reveal that a small number of attention heads located in the later layers of the vision encoder are responsible for the effectiveness of typographic attacks. By selectively ablating a typographic circuit, Dyslexify is able to defend CLIP against typographic attacks without requiring fine-tuning steps, offering a practical and interpretable method for controlling model behavior. To our knowledge, this is the first work to address typographic attacks in CLIP through causal interventions. Dyslexify demonstrates that fine-grained control over model capabilities is achievable through targeted architectural manipulations *without* retraining, and thus paves the way for more robust and modular deployment of multimodal models. Beyond standard benchmarks, we further show that typographic attacks constitute a realistic threat vector in the medical domain, where they can mislead safety-critical models, and that Dyslexify substantially mitigates this vulnerability. We believe this work motivates a broader shift toward mechanistic interpretability as a tool not only for understanding, but for controlling safety-relevant behaviors in deep transformer models. Finally, we release a family of dyslexic CLIP models that are significantly more robust against typographic attacks. These models serve as drop-in replacements for safety-critical applications where the risks posed by adversarial text manipulation outweigh the benefits of typographic understanding.

**Limitations and future work:** Dyslexify enhances the typographic robustness of the `cls` token by preventing specialized typographic attention heads from writing to it. However, many multimodal applications, such as LLaVA and IP adapters (Ye et al., 2023; Liu et al., 2023; 2024b), leverage not only the `cls` token but also spatial tokens, allowing typographic information to propagate into downstream tasks. This might limit the impact of Dyslexify on improving robustness in applications, and calls for further investigation into its generalizability to VLM setups.

Furthermore, it is standard practice to evaluate adversarial defenses against adaptive attacks (Tramer et al., 2020), i.e., attacks that are explicitly optimized to circumvent the defense mechanism. In our case, however, such an evaluation is not feasible: typographic attacks are inherently non-differentiable, which prevents constructing adaptive variants that directly optimize against Dyslexify.

**Misuse Potential:** While we aim to enhance the safety of multimodal systems, we acknowledge that our insights into CLIP’s behavior under typographic attacks could be exploited by attackers. Specifically, adversarial inputs might be crafted to increase the spatial attention of heads in  $\mathcal{C}$ , making typographic attacks even more effective.

486 ETHICS STATEMENT  
487488 We affirm that this work adheres to the **ICLR Code of Ethics**. All authors have read and agree with  
489 the Code. We note that our study does not involve human subjects or sensitive personal data. While  
490 insights into typographic attacks may inform adversarial strategies, our primary aim is to strengthen  
491 robustness and safety of multimodal models.  
492493 REPRODUCIBILITY STATEMENT  
494495 We have taken efforts to make our results reproducible. Our code is open-sourced and provided to  
496 reviewers in anonymized form. All results and the majority of plots in the paper can be reproduced  
497 with the released code.  
498499 REFERENCES  
500

501 Hiroki Azuma and Yusuke Matsui. Defense-prefix for preventing typographic attacks on clip. In *Proceedings of the IEEE/CVF International Conference on Computer Vision*, pp. 3644–3653, 2023.

502 Lukas Bossard, Matthieu Guillaumin, and Luc Van Gool. Food-101–mining discriminative components with random forests. In *Computer vision–ECCV 2014: 13th European conference, zurich, Switzerland, September 6–12, 2014, proceedings, part VI 13*, pp. 446–461. Springer, 2014.

503 G. Bradski. The OpenCV Library. *Dr. Dobb’s Journal of Software Tools*, 2000.

504 Yue Cao, Yun Xing, Jie Zhang, Di Lin, Tianwei Zhang, Ivor Tsang, Yang Liu, and Qing Guo. Scenetap: Scene-coherent typographic adversarial planner against vision-language models in  
505 real-world environments. *arXiv preprint arXiv:2412.00114*, 2024.

506 Hao Cheng, Erjia Xiao, Jiayan Yang, Jiahang Cao, Qiang Zhang, Jize Zhang, Kaidi Xu, Jindong  
507 Gu, and Renjing Xu. Uncovering vision modality threats in image-to-image tasks. *arXiv preprint  
508 arXiv:2412.05538*, 2024.

509 Noel CF Codella, David Gutman, M Emre Celebi, Brian Helba, Michael A Marchetti, Stephen W  
510 Dusza, Aadi Kalloo, Konstantinos Liopyris, Nabin Mishra, Harald Kittler, et al. Skin lesion analysis  
511 toward melanoma detection: A challenge at the 2017 international symposium on biomedical  
512 imaging (isbi), hosted by the international skin imaging collaboration (isic). In *2018 IEEE 15th  
513 international symposium on biomedical imaging (ISBI 2018)*, pp. 168–172. IEEE, 2018.

514 Marc Combalia, Noel CF Codella, Veronica Rotemberg, Brian Helba, Veronica Vilaplana, Ofer Reiter,  
515 Cristina Carrera, Alicia Barreiro, Allan C Halpern, Susana Puig, et al. Bcn20000: Dermoscopic  
516 lesions in the wild. *arXiv preprint arXiv:1908.02288*, 2019.

517 Cheng Cui, Ting Sun, Manhui Lin, Tingquan Gao, Yubo Zhang, Jiaxuan Liu, Xueqing Wang, Zelun  
518 Zhang, Changda Zhou, Hongen Liu, Yue Zhang, Wenyu Lv, Kui Huang, Yichao Zhang, Jing  
519 Zhang, Jun Zhang, Yi Liu, Dianhai Yu, and Yanjun Ma. Paddleocr 3.0 technical report, 2025. URL  
<https://arxiv.org/abs/2507.05595>.

520 Jia Deng, Wei Dong, Richard Socher, Li-Jia Li, Kai Li, and Li Fei-Fei. Imagenet: A large-scale  
521 hierarchical image database. In *2009 IEEE conference on computer vision and pattern recognition*,  
522 pp. 248–255. Ieee, 2009.

523 Maximilian Dreyer, Lorenz Hufe, Jim Berend, Thomas Wiegand, Sebastian Lapuschkin, and Wojciech  
524 Samek. From what to how: Attributing clip’s latent components reveals unexpected semantic  
525 reliance. *arXiv preprint arXiv:2505.20229*, 2025.

526 Sedigheh Eslami, Christoph Meinel, and Gerard De Melo. Pubmedclip: How much does clip benefit  
527 visual question answering in the medical domain? In *Findings of the Association for Computational  
528 Linguistics: EACL 2023*, pp. 1151–1163, 2023.

529 Gabriel Goh, Nick Cammarata, Chelsea Voss, Shan Carter, Michael Petrov, Ludwig Schubert, Alec  
530 Radford, and Chris Olah. Multimodal neurons in artificial neural networks. *Distill*, 2021. doi:  
531 10.23915/distill.00030. <https://distill.pub/2021/multimodal-neurons>.

540 Yichen Gong, Delong Ran, Jinyuan Liu, Conglei Wang, Tianshuo Cong, Anyu Wang, Sisi Duan, and  
 541 Xiaoyun Wang. Figstep: Jailbreaking large vision-language models via typographic visual prompts.  
 542 In *Proceedings of the AAAI Conference on Artificial Intelligence*, volume 39, pp. 23951–23959,  
 543 2025.

544 Kuo-Han Hung, Ching-Yun Ko, Ambrish Rawat, I Chung, Winston H Hsu, Pin-Yu Chen, et al.  
 545 Attention tracker: Detecting prompt injection attacks in llms. *arXiv preprint arXiv:2411.00348*,  
 546 2024.

548 Gabriel Ilharco, Mitchell Wortsman, Ross Wightman, Cade Gordon, Nicholas Carlini, Rohan Taori,  
 549 Achal Dave, Vaishaal Shankar, Hongseok Namkoong, John Miller, Hannaneh Hajishirzi, Ali  
 550 Farhadi, and Ludwig Schmidt. Openclip, July 2021. URL <https://doi.org/10.5281/zenodo.5143773>.

552 Gabriel Ilharco, Mitchell Wortsman, Samir Yitzhak Gadre, Shuran Song, Hannaneh Hajishirzi, Simon  
 553 Kornblith, Ali Farhadi, and Ludwig Schmidt. Patching open-vocabulary models by interpolating  
 554 weights. *Advances in Neural Information Processing Systems*, 35:29262–29277, 2022.

556 Sonia Joseph, Praneet Suresh, Ethan Goldfarb, Lorenz Hufe, Yossi Gandelsman, Robert Graham,  
 557 Danilo Bzdok, Wojciech Samek, and Blake Aaron Richards. Steering clip’s vision transformer  
 558 with sparse autoencoders. *arXiv preprint arXiv:2504.08729*, 2025.

559 Subaru Kimura, Ryota Tanaka, Shumpei Miyawaki, Jun Suzuki, and Keisuke Sakaguchi. Empirical  
 560 analysis of large vision-language models against goal hijacking via visual prompt injection. *arXiv  
 561 preprint arXiv:2408.03554*, 2024.

563 Xiang Li, Congcong Wen, Yuan Hu, and Nan Zhou. Rs-clip: Zero shot remote sensing scene  
 564 classification via contrastive vision-language supervision. *International Journal of Applied Earth  
 565 Observation and Geoinformation*, 124:103497, 2023.

566 Fan Liu, Delong Chen, Zhangqingyun Guan, Xiaocong Zhou, Jiale Zhu, Qiaolin Ye, Liyong Fu, and  
 567 Jun Zhou. Remoteclip: A vision language foundation model for remote sensing. *IEEE Transactions  
 568 on Geoscience and Remote Sensing*, 62:1–16, 2024a.

569 Haotian Liu, Chunyuan Li, Qingsong Wu, and Yong Jae Lee. Visual instruction tuning, 2023.

571 Haotian Liu, Chunyuan Li, Yuheng Li, Bo Li, Yuanhan Zhang, Sheng Shen, and Yong Jae Lee.  
 572 Llava-next: Improved reasoning, ocr, and world knowledge, January 2024b. URL <https://llava-vl.github.io/blog/2024-01-30-llava-next/>.

575 Mingrui Liu, Sixiao Zhang, and Cheng Long. Wukong framework for not safe for work detection in  
 576 text-to-image systems. *arXiv preprint arXiv:2508.00591*, 2025.

577 S. Maji, J. Kannala, E. Rahtu, M. Blaschko, and A. Vedaldi. Fine-grained visual classification of  
 578 aircraft. Technical report, 2013.

580 Joanna Materzyńska, Antonio Torralba, and David Bau. Disentangling visual and written concepts in  
 581 clip. In *Proceedings of the IEEE/CVF Conference on Computer Vision and Pattern Recognition*,  
 582 pp. 16410–16419, 2022.

583 A. Mishra, K. Alahari, and C. V. Jawahar. Scene text recognition using higher order language priors.  
 584 In *BMVC*, 2012.

586 Maan Qraitem, Nazia Tasnim, Piotr Teterwak, Kate Saenko, and Bryan A Plummer. Vision-llms can  
 587 fool themselves with self-generated typographic attacks. *arXiv preprint arXiv:2402.00626*, 2024.

588 Alec Radford, Jong Wook Kim, Chris Hallacy, Aditya Ramesh, Gabriel Goh, Sandhini Agarwal,  
 589 Girish Sastry, Amanda Askell, Pamela Mishkin, Jack Clark, et al. Learning transferable visual  
 590 models from natural language supervision. In *International conference on machine learning*, pp.  
 591 8748–8763. PMLR, 2021.

593 Camilo Carvajal Reyes, Joaquín Fontbona, and Felipe Tobar. Towards sfw sampling for diffusion  
 594 models via external conditioning. *arXiv preprint arXiv:2505.08817*, 2025.

594    Christoph Schuhmann, Romain Beaumont, Richard Vencu, Cade Gordon, Ross Wightman, Mehdi  
 595    Cherti, Theo Coombes, Aarush Katta, Clayton Mullis, Mitchell Wortsman, et al. Laion-5b: An  
 596    open large-scale dataset for training next generation image-text models. *Advances in neural*  
 597    *information processing systems*, 35:25278–25294, 2022.

598    Florian Tramer, Nicholas Carlini, Wieland Brendel, and Aleksander Madry. On adaptive attacks to  
 599    adversarial example defenses. *Advances in neural information processing systems*, 33:1633–1645,  
 600    2020.

602    Philipp Tschandl, Cliff Rosendahl, and Harald Kittler. The ham10000 dataset, a large collection of  
 603    multi-source dermatoscopic images of common pigmented skin lesions. *Scientific data*, 5(1):1–9,  
 604    2018.

605    Vicente Vivanco, Gaurav Kumar Nayak, and Mubarak Shah. Geoclip: Clip-inspired alignment  
 606    between locations and images for effective worldwide geo-localization. In *Advances in Neural*  
 607    *Information Processing Systems*, 2023.

609    Zifeng Wang, Zhenbang Wu, Dinesh Agarwal, and Jimeng Sun. Medclip: Contrastive learning from  
 610    unpaired medical images and text. In *Proceedings of the Conference on Empirical Methods in*  
 611    *Natural Language Processing. Conference on Empirical Methods in Natural Language Processing*,  
 612    volume 2022, pp. 3876, 2022.

613    Justus Westerhoff, Erblina Purellku, Jakob Hackstein, Leo Pinetzki, and Lorenz Hufe. Scam: A  
 614    real-world typographic robustness evaluation for multimodal foundation models. *arXiv preprint*  
 615    *arXiv:2504.04893*, 2025.

616    Guangxuan Xiao, Yuandong Tian, Beidi Chen, Song Han, and Mike Lewis. Efficient streaming  
 617    language models with attention sinks. *arXiv preprint arXiv:2309.17453*, 2023.

619    Yue Yang, Mona Gandhi, Yufei Wang, Yifan Wu, Michael Yao, Chris Callison-Burch, James Gee,  
 620    and Mark Yatskar. A textbook remedy for domain shifts: Knowledge priors for medical image  
 621    analysis. *Advances in neural information processing systems*, 37:90683–90713, 2024.

623    Hu Ye, Jun Zhang, Sibo Liu, Xiao Han, and Wei Yang. Ip-adapter: Text compatible image prompt  
 624    adapter for text-to-image diffusion models. *arXiv preprint arXiv:2308.06721*, 2023.

625  
 626  
 627  
 628  
 629  
 630  
 631  
 632  
 633  
 634  
 635  
 636  
 637  
 638  
 639  
 640  
 641  
 642  
 643  
 644  
 645  
 646  
 647

648	CONTENTS OF APPENDIX	
649		
650		
651	<b>A Use of Large Language Models</b>	13
652		
653	<b>B MLP layers compress information</b>	13
654		
655	<b>C Attention sinks for typographic attention heads</b>	14
656		
657	<b>D Ablation Curves</b>	15
658		
659	<b>E Further details on Medical Application</b>	16
660		
661	<b>F Datasets</b>	17
662		
663	<b>G Circuit size</b>	17
664		
665	<b>H OCR capabilities</b>	17
666		
667	<b>I Runtime and memory requirements</b>	18
668		
669	<b>J Blurring baseline</b>	18
670		
671	<b>K Relationship between probes and <math>T_{i,\ell}</math> scores</b>	19
672		

## A USE OF LARGE LANGUAGE MODELS

Large Language Models (LLMs) were used in the preparation of this work. Specifically, they assisted in polishing the text, generating code snippets, and conducting literature searches. All conceptual contributions, experimental designs, analyses, and conclusions are the sole work of the authors.

## B MLP LAYERS COMPRESS INFORMATION

In Section 3, we observe that  $\text{Acc}(P_{\text{img},\ell})$  and  $\text{Acc}(P_{\text{typo},\ell})$  increases after attention layers, but consistently drops following MLP blocks. Thus we estimate the intrinsic dimensionality (ID) of `cls`-token representations across layers using PCA. From a 5% split of the ImageNet-100-Typo training set, we extract residual stream activations for each layer. For each embedding  $h_\ell \in \mathbb{R}^d$ , we fit PCA and define ID as the smallest number of principal components  $k$  such that the cumulative explained variance exceeds 95%:

$$\text{ID} = \min \left\{ k : \frac{\sum_{j=1}^k \lambda_j}{\sum_{j=1}^d \lambda_j} \geq 0.95 \right\},$$

where  $\lambda_j$  are the PCA eigenvalues. A larger ID indicates higher representational complexity. We report ID across layers and token types to analyze how typographic inputs affect the geometry of CLIP representations.

**Results** Fig. 7 compares linear probe accuracy (left) and ID (right) across layers of a ViT-B model. We observe a consistent pattern: attention layers tend to increase both probe accuracy and intrinsic dimensionality, while MLP layers reduce them. This trend is most prominent in the middle layers (3–7), suggesting that attention blocks introduce linearly accessible information, whereas MLPs compress or remove it.

This pattern is not consistent throughout the model. The MLPs at layers 9 and 11 exhibit increases in ID, deviating from the overall compression trend. Conversely, the attention block at layer 11 causes a sharp drop in ID. These exceptions indicate that deeper layers may serve more specialized roles.

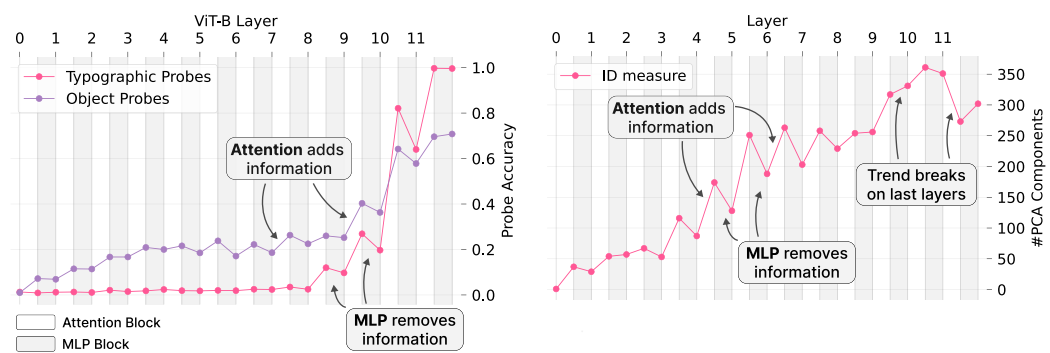
702  
703

Attention Layers add information to the CLS tokens, while MLPs remove information from it

704

a) This can be observed in the probe accuracy

705



706

707

708

709

710

711

712

713

714

715

716

717

Figure 7: Attention layers increase, MLP layers reduce `cls` token information. **(a)** Linear probe accuracy rises after attention blocks and drops after MLPs, indicating improved linear accessibility followed by compression. **(b)** Intrinsic dimensionality shows a matching trend, especially in layers 3–7. Exceptions include MLPs at layers 9 and 11 (ID increase) and the attention block at layer 11 (ID drop), suggesting deeper-layer specialization.

718

719

720

721

722

723

724

### C ATTENTION SINKS FOR TYPOGRAPHIC ATTENTION HEADS

725

726

727

728

729

730

731

732

733

734

735

We analyze the attention patterns of head 5 in layer 6 ( $\mathcal{H}_{5,6}$ ) in ViT-B, which has the highest  $T_{i,\ell}$  score in the model. More specifically we evaluate its spatial attention norm  $\|A_{5,6}^*\|$  on ImageNet-100 and ImageNet-100-Typo. As shown in Fig. 8,  $\|A_{5,6}^*\|$  is systematically higher on ImageNet-100-Typo than on ImageNet-100. While the distribution on typographic images is unimodal, the distribution on the original dataset is bimodal. Manual inspection reveals that the high-norm mode in ImageNet-100 contains incidental text in, such as watermarks or copyright tags.

One possible interpretation of these results is that  $\mathcal{H}_{5,6}$  uses the `cls`-to-`cls` attention as an attention sink (Xiao et al., 2023), to selectively adjust the impact of this specialized typographic attention head.

Building on these findings we evaluate  $\mathcal{H}_{5,6}$ ’s capabilities to predict if a sample  $x$  originates from ImageNet-100 or ImageNet-100-typo. The score  $\|A_{5,6}^*\|$  ROC-AUC of 0.887, indicating that this attention signal can be used as a robust classifier. In comparison, a linear classifier trained on the same task reaches an ROC-AUC of 1.0, but overfits to superficial typographic features specific to the ImageNet-100-Typo construction. Many images in the original dataset that contain real-world typography are still correctly classified as non-typographic by this probe - supporting the conclusion that it does not generalize beyond the synthetic intervention.

743

744

745

746

747

748

749

750

751

752

753

754

755

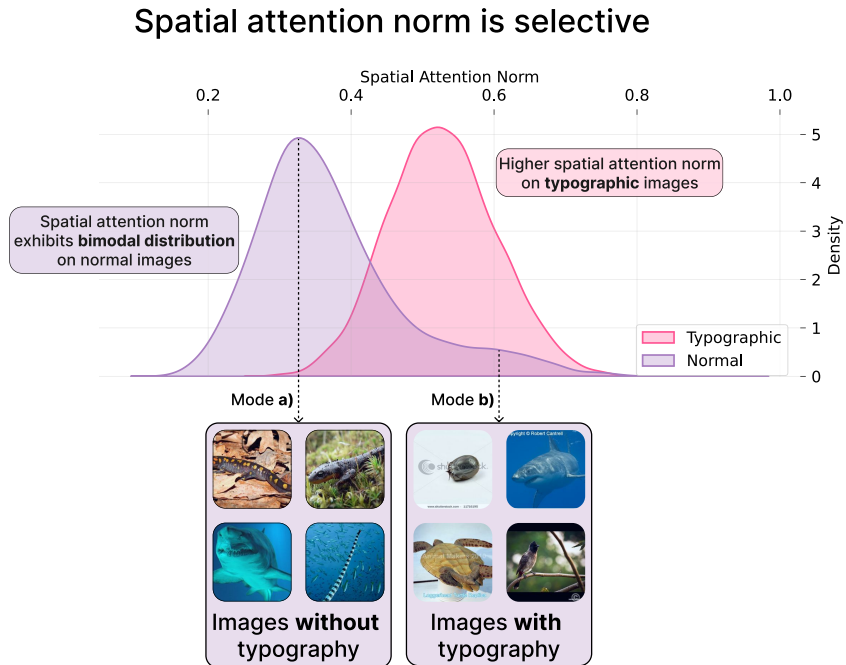


Figure 8: Distribution of the spatial attention norm of ViT-B head  $\mathcal{H}_{5,6}$  across ImageNet-100 and ImageNet-100-Typo. The norm is consistently higher for typographic images, while the non-typographic distribution is bimodal. Manual inspection links the higher mode to incidental text, suggesting that the head selectively activates in response to typography, regardless of its origin.

## D ABLATION CURVES

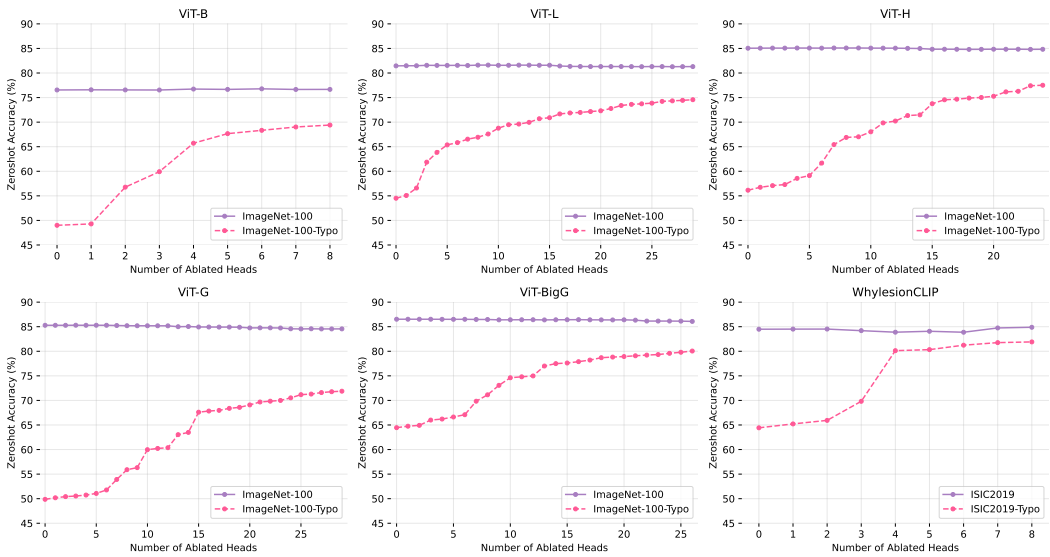


Figure 9: Tradeoff between general accuracy and typographic robustness as a function of the number of ablated heads. Ablations are applied in decreasing order of  $T_{i,\ell}$ .

810 E FURTHER DETAILS ON MEDICAL APPLICATION  
811

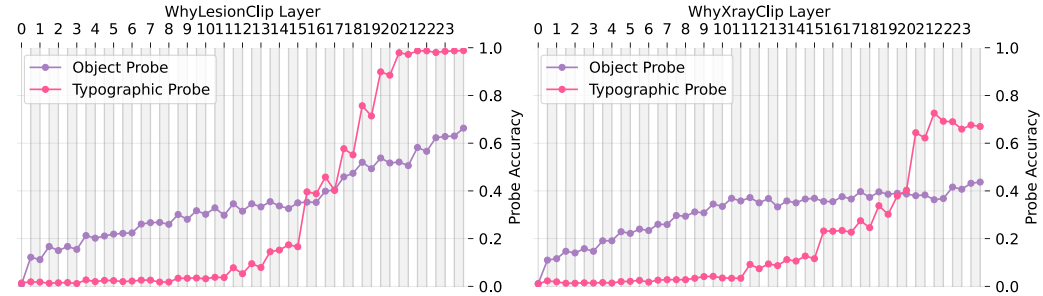
812 We evaluated Dyslexify in the safety-critical context of melanoma detection, using WhyLesionCLIP  
813 based on OpenCLIP ViT-L as the underlying foundation model. To construct typographic attack  
814 datasets, we introduced textual labels into ISIC2019, HAM10k, and BCN20k, resulting in paired  
815 typographic variants. The typographic circuit was selected using the same procedure as in Section 5.2,  
816 with tolerance  $\epsilon = 0.01$  and maximum skips  $k = 10$ .

817 Table 4 reports detailed results. We find that typographic attacks reduce zero-shot accuracy by  
818 up to 22.1%, while Dyslexify recovers up to 19.3% accuracy, and even improves performance on  
819 non-attacked datasets in some cases. These results confirm that typographic attacks pose a realistic  
820 failure mode for medical AI systems.

821 Fig. 10 further illustrates that typographic probes perform more strongly in WhyXrayCLIP than  
822 in WhyLesionCLIP, which may be explained by frequent typographic artifacts (e.g., “R” markers)  
823 in X-ray training data. This suggests that the degree of vulnerability depends on the presence of  
824 typographic features in the training distribution.

825  
826 Table 4: Comparison of dyslexic model performance on WhyLesionCLIP dataset, showing accuracy  
827 changes relative to the base model, with improvements ( $\uparrow$ ) or declines ( $\downarrow$ ). The suffix -T indicates the  
828 corresponding typographic version of the dataset.

830 831 Model	Not Typographic				Synthetic Typographic			
	ISIC2019	Melanoma	BCN20k	HAM10k	ISIC2019-T	Melanoma-T	BCN20k-T	HAM10k-T
832 Base	77.80	84.10	31.99	35.66	55.19	62.10	19.65	19.48
833 Ours	77.47 $\downarrow 0.33$	84.40 $\uparrow 0.30$	32.49 $\uparrow 0.50$	40.20 $\uparrow 4.54$	70.92 $\uparrow 15.73$	81.40 $\uparrow 19.30$	26.46 $\uparrow 6.81$	24.42 $\uparrow 4.94$

835  
836 a) Typographic probes perform more strongly in the lesion model than in the xray model837  
838 b) Typographic artifacts in training data (e.g., R-markers) may explain robustness

839 Figure 10: (a) Linear probes on CLS embeddings show that typographic probes perform less well in  
840 WhyLesionCLIP compared to WhyXrayCLIP, indicating weaker encoding of typographic features  
841 in the lesion model. (b) Examples of typographic artifacts (e.g., “R” markers) commonly found in  
842 X-ray training data, which may influence probe performance.

864 **F DATASETS**  
865866 For the zero-shot evaluation we tested a variety of datasets, grouped below by purpose.  
867868 **RTA-100** (Azuma & Matsui, 2023) consists of 1,000 handcrafted typographic attacks, each written  
869 on a Post-it note and overlaid onto natural images.870 **Disentangling** (Materzyńska et al., 2022) includes 180 typographic attacks, also written on Post-its,  
871 designed to probe the separation of visual and textual features in multimodal models.872 **PAINT-DS** (Ilharco et al., 2022) comprises 110 Post-it-based typographic attacks and serves to  
873 evaluate patch-level vulnerabilities in vision-language models.874 **Food-101** (Bossard et al., 2014) is a standard image classification dataset containing 101 food  
875 categories, each with 1,000 images.876 **FGVC-Aircraft** (Maji et al., 2013) (referred to as *Aircraft* in our paper) is a fine-grained classification  
877 benchmark consisting of 10,000 images across 100 aircraft variants.878 **ImageNet-100**<sup>2</sup> is a subset of the ImageNet-1k dataset (Deng et al., 2009), containing 100 object and  
879 animal classes with 1,000 images per class.880 **ISIC2019**<sup>3</sup> contains 25,331 images available for the classification of dermoscopic images among  
881 nine different diagnostic Tschandl et al. (2018); Combalia et al. (2019); Codella et al. (2018). In this  
882 paper we evaluate the binary classification task into the classes "Benign" and "Malignant".883 **HAM10k** (Tschandl et al., 2018) includes 10,015 dermatoscopic images labeled into seven diagnostic  
884 categories: *Actinic Keratoses*, *Basal Cell Carcinoma*, *Benign Keratosis-like Lesions*, *Dermatofibroma*,  
885 *Melanoma*, *Melanocytic Nevi*, and *Vascular Lesions*.886 **BCN20k** (Combalia et al., 2019) comprises 19,424 dermatoscopic images collected at the Hospital  
887 Clínic de Barcelona, annotated into eight categories: *Actinic Keratoses*, *Basal Cell Carcinoma*, *Benign*  
888 *Keratosis-like Lesions*, *Dermatofibroma*, *Melanocytic Nevi*, *Melanoma*, *Squamous Cell Carcinoma*,  
889 and *Vascular Lesions*.890 For the generation of the -typo dataset we used the following fonts: Times New Roman, Georgia,  
891 Arial.  
892893 **G CIRCUIT SIZE**  
894895 Table 5: Number of selected and total heads  $\mathcal{H}_{i,\ell}$  in circuit  $\mathcal{C}$  per model

Model	Selected	Total	Percentage (%)
B	8	144	5.6
L	29	288	10.1
H	24	384	6.2
G	29	480	6.0
Big-G	26	576	4.5

900 **H OCR CAPABILITIES**  
901902 Dyslexify is designed to suppress typographic understanding in favor of robustness to typographic  
903 attacks. As a consequence, we expect a degradation on tasks that require optical character recognition  
904 (OCR).905 To quantify this effect, we evaluate the base and dyslexic OpenCLIP models on the IIIT5K word  
906 recognition benchmark (Mishra et al., 2012), using the standard small and medium lexicon settings.907  
908 <sup>2</sup><https://www.kaggle.com/datasets/ambityga/imagenet100>909 <sup>3</sup><https://www.kaggle.com/datasets/salvioxhexia/isic-2019-skin-lesion-images-for-classification>

918 For each image, we treat the lexicon entries as candidate labels and perform zero-shot classification  
 919 with CLIP, reporting the top-1 word accuracy.  
 920

921 Table 6 reports the results. Across all model sizes, Dyslexify substantially reduces OCR performance,  
 922 with drops between 8 and 30 percentage points depending on the model and lexicon size. The effect  
 923 is strongest for the smaller ViT-B and ViT-L models and remains pronounced even for the larger  
 924 ViT-bigG.

925 This confirms that dyslexic models are not appropriate for applications that benefit from text recogni-  
 926 tion. Instead, they are intended as drop-in replacements in safety-critical settings where the risks of  
 927 adversarial text manipulation outweigh the utility of typographic understanding.

929 Table 6: Comparison of dyslexic model performance on IIIT5K OCR evaluation, showing accuracy  
 930 changes relative to the base model, with improvements ( $\uparrow$ ) or declines ( $\downarrow$ ).

Model	Small Lexicon	Medium Lexicon
B	25.03 $\downarrow$ 30.50	11.37 $\downarrow$ 17.87
L	35.50 $\downarrow$ 30.27	15.30 $\downarrow$ 20.47
H	51.27 $\downarrow$ 12.23	26.40 $\downarrow$ 8.57
G	51.40 $\downarrow$ 13.70	27.27 $\downarrow$ 10.03
Big-G	54.47 $\downarrow$ 20.37	29.40 $\downarrow$ 15.67

## I RUNTIME AND MEMORY REQUIREMENTS

942 We benchmark the computational cost of Dyslexify against Defense-Prefix (DP) in terms of wall-clock  
 943 runtime and memory requirements. All experiments were run on a single NVIDIA H200 GPU using  
 944 identical data pipelines and batch sizes. Importantly, both methods were evaluated using the *entire*  
 945 *ImageNet-100 training split* for circuit construction and prefix optimization, respectively.

947 Table 7: Runtime comparison of Dyslexify and Defense-Prefix (DP) in seconds on a single NVIDIA  
 948 H200 GPU. Lower is better.

Model	Dyslexify	DP
ViT-B	3 818	14 598
ViT-L	23 518	23 145
ViT-H	24 237	39 483

954 Dyslexify is  $3.8 \times$  faster than DP on ViT-B,  $1.6 \times$  faster on ViT-H, and comparable on ViT-L. The  
 955 cost gap reflects the fact that Dyslexify requires only forward passes with circuit ablations, whereas  
 956 DP performs gradient-based optimization over a learnable prefix.  
 957

958 **Runtime reduction through subset evaluation.** The reported Dyslexify runtimes use the *full*  
 959 ImageNet-100 training set. In practice, Dyslexify does not require the entire dataset: we observe that  
 960 using a significantly smaller random subset yields nearly identical circuits and comparable robustness  
 961 gains.  
 962

963 **VRAM requirements.** Dyslexify further has a low memory footprint. It runs on all evaluated  
 964 models, including those exceeding 1B parameters, on a single NVIDIA Titan RTX (24 GB). Defense-  
 965 Prefix cannot be trained beyond ViT-L due to CUDA out-of-memory errors. This makes Dyslexify  
 966 suitable for low-resource environments where finetuning-based defenses are infeasible.  
 967

## J BLURRING BASELINE

971 Following the reviewer’s suggestion, we implemented a simple OCR-based defense baseline that  
 removes typographic content directly from the image. We use the PaddleOCR text detector (Cui et al.,

972 2025) to localize text regions and then apply a Gaussian blur to each detected bounding box using  
 973 OpenCV (Bradski, 2000)..  
 974

975 In brief, for each input image we (1) run an OCR pass to obtain polygonal text boxes; (2) compute the  
 976 pixel bounds of each box; and (3) blur only the corresponding subregion with a large-kernel Gaussian  
 977 filter (kernel size 51,  $\sigma = 25$ ). No other pixels are modified. This produces a text-ablated variant of  
 978 ImageNet-100-Typo that preserves the underlying image content while suppressing overlaid words.  
 979

980 This baseline allows direct comparison between Dyslexify (a mechanistic intervention) and a purely  
 981 image-level text-removal defense.

982 The OCR+blur baseline is strong: it consistently outperforms Dyslexify on ImageNet-100-Typo  
 983 across all model sizes. This confirms that removing text at the pixel level is an effective strategy for  
 984 mitigating typographic attacks. On non-typographic datasets, the blur baseline has minimal impact -  
 985 the accuracy remains within  $\pm 0.3\%$  of the original models - indicating that the image modifications  
 986 do not substantially harm object-centric features. Dyslexify shows similarly small degradation (<1%),  
 987 but delivers lower absolute robustness than OCR+blur on this benchmark.

988 While OCR-based preprocessing is competitive in absolute robustness, it comes with clear limita-  
 989 tions. First, OCR+blur must be applied at every inference step, adding recurring computational  
 990 overhead, whereas Dyslexify is executed once per model and introduces no inference-time cost.  
 991 Second, OCR+blur removes visual information rather than modifying internal causal pathways; it  
 992 therefore does not provide mechanistic insight into model behavior or contribute to understanding the  
 993 underlying failure modes.

994 Overall, the results highlight that OCR-based preprocessing is a strong baseline, but Dyslexify serves  
 995 a different purpose: it demonstrates that mechanistic analysis can yield actionable interventions that  
 996 improve robustness without retraining and without modifying the input image.

997 We hope that this comparison highlights a broader point: while preprocessing-based defenses can  
 998 be strong, they do not replace the need for mechanistic approaches. Our results show that even  
 999 simple circuit-level interventions can yield meaningful robustness gains without retraining, without  
 1000 modifying inputs, and without inference-time overhead. We hope that this work encourages further  
 1001 research on actionable interpretability - using mechanistic understanding not only to analyze models,  
 1002 but to directly improve their safety and reliability.

1003 1004 Table 8: Comparison of dyslexic model performance on ImageNet-100 with and without blur.

ImageNet-100	B	L	H	G	Big-G
Normal	74.36	<b>79.76</b>	<u>83.74</u>	<b>83.24</b>	<b>85.06</b>
Blurred	74.32	79.48	<b>83.88</b>	<u>83.20</u>	84.94
Dyslexify	<b>75.00</b>	<u>79.52</u>	83.40	82.58	84.72
Both	<u>74.64</u>	79.50	83.50	82.52	84.60

1011 1012 1013 Table 9: Comparison of dyslexic model performance on ImageNet-100-Typo with and without blur.

ImageNet-100-Typo	B	L	H	G	Big-G
Normal	46.94	51.90	54.08	46.70	61.90
Blurred	<b>68.52</b>	<b>75.12</b>	<u>79.98</u>	<b>79.56</b>	<b>80.84</b>
Dyslexify	66.84	72.22	75.34	68.76	78.64
Both	<u>67.86</u>	<u>74.30</u>	<b>80.00</b>	<u>78.48</u>	<u>80.52</u>

## 1020 1021 1022 K RELATIONSHIP BETWEEN PROBES AND $T_{i,\ell}$ SCORES

1023 As discussed in Section 3, we observe a strong correspondence between layers with elevated  $T_{i,\ell}$   
 1024 scores and those where the typographic probe  $P_{\text{typo},\ell}$  exhibits sharp increases in accuracy. In this  
 1025 section, we extend this analysis across all evaluated model sizes to support the trends previously

1026 shown for ViT-B. Fig. 11 to Fig. 15 visualize this relationship for each model. To improve readability,  
 1027 we transpose the probe accuracy plots: the  $y$ -axis denotes the layer index, while the  $x$ -axis indicates  
 1028 probe accuracy.  
 1029

1030

1031

1032

1033

1034

1035

1036

1037

1038

1039

1040

1041

1042

1043

1044

1045

1046

1047

1048

1049

1050

1051

1052

1053

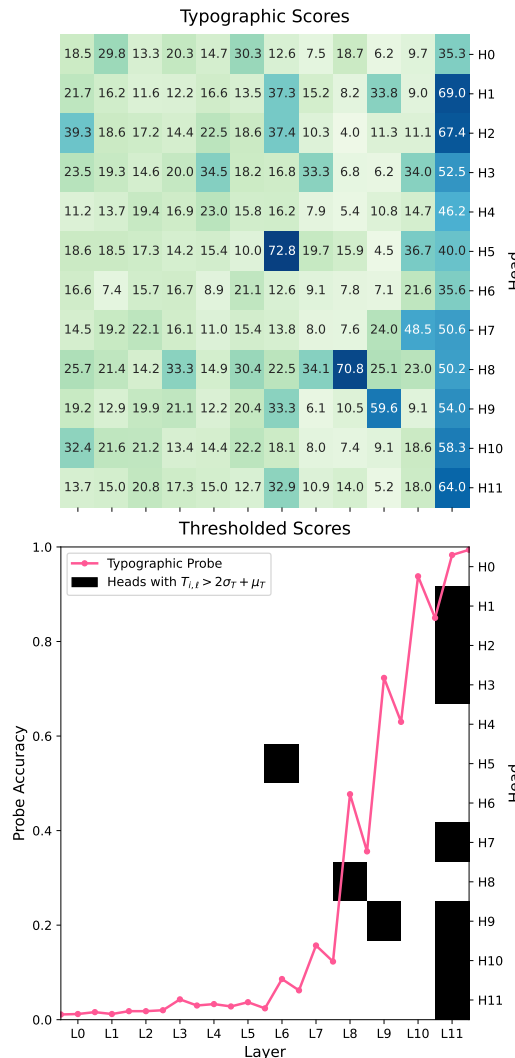
1054

1055

1056

1057

1058



1076 Figure 11: ViT-B typographic attention scores  $T_{i,l}$  (top), thresholded and compared with linear  
 1077 probe accuracies (bottom). Layers with higher typographic attention scores align with increased  
 1078 probe accuracy, highlighting a correspondence between attention patterns and typographic feature  
 1079 decodability.

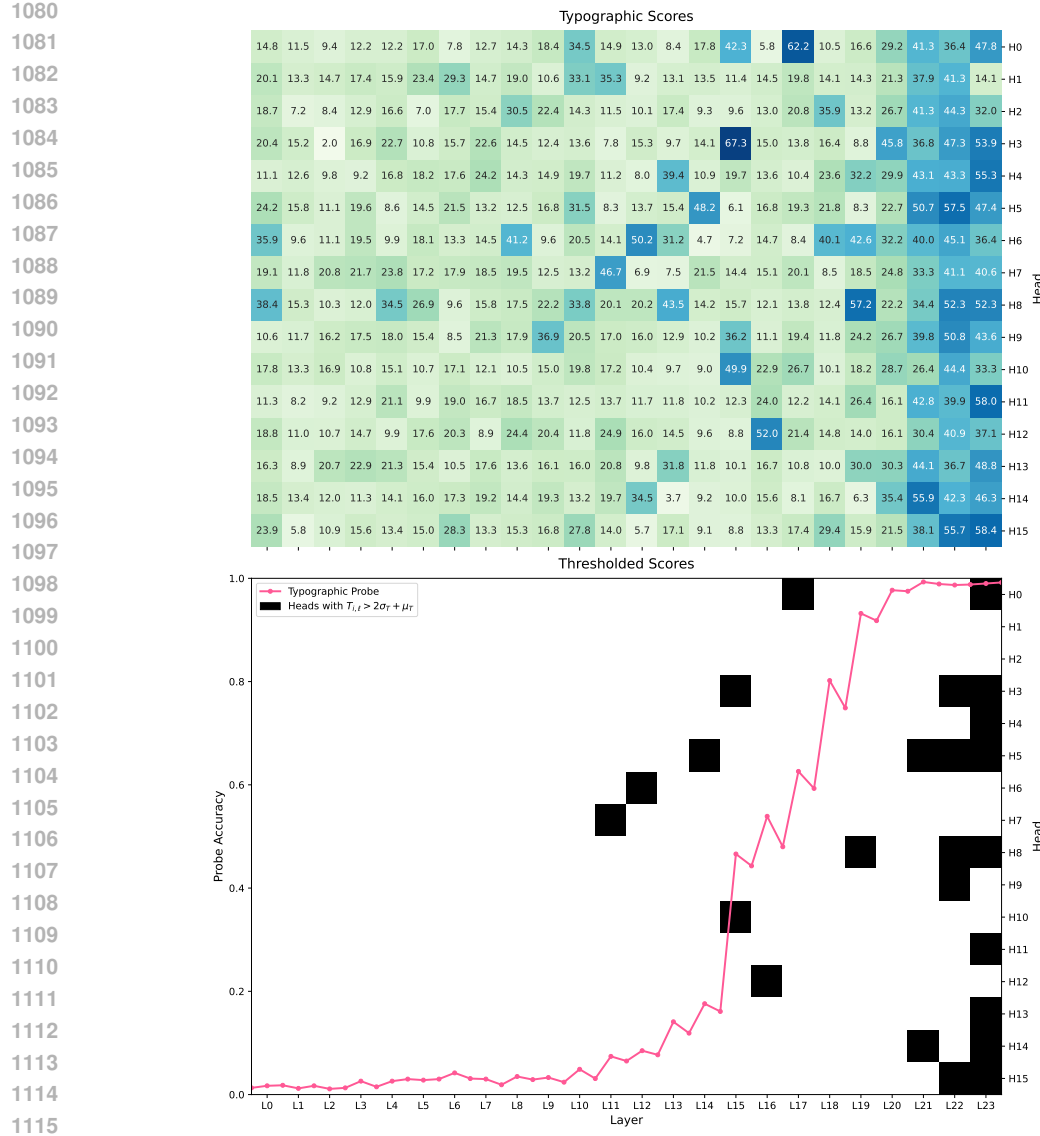


Figure 12: ViT-L typographic attention scores  $T_{i,\ell}$  (top), thresholded and compared with linear probe accuracies (bottom). Layers with higher typographic attention scores align with increased probe accuracy, highlighting a correspondence between attention patterns and typographic feature decodability.

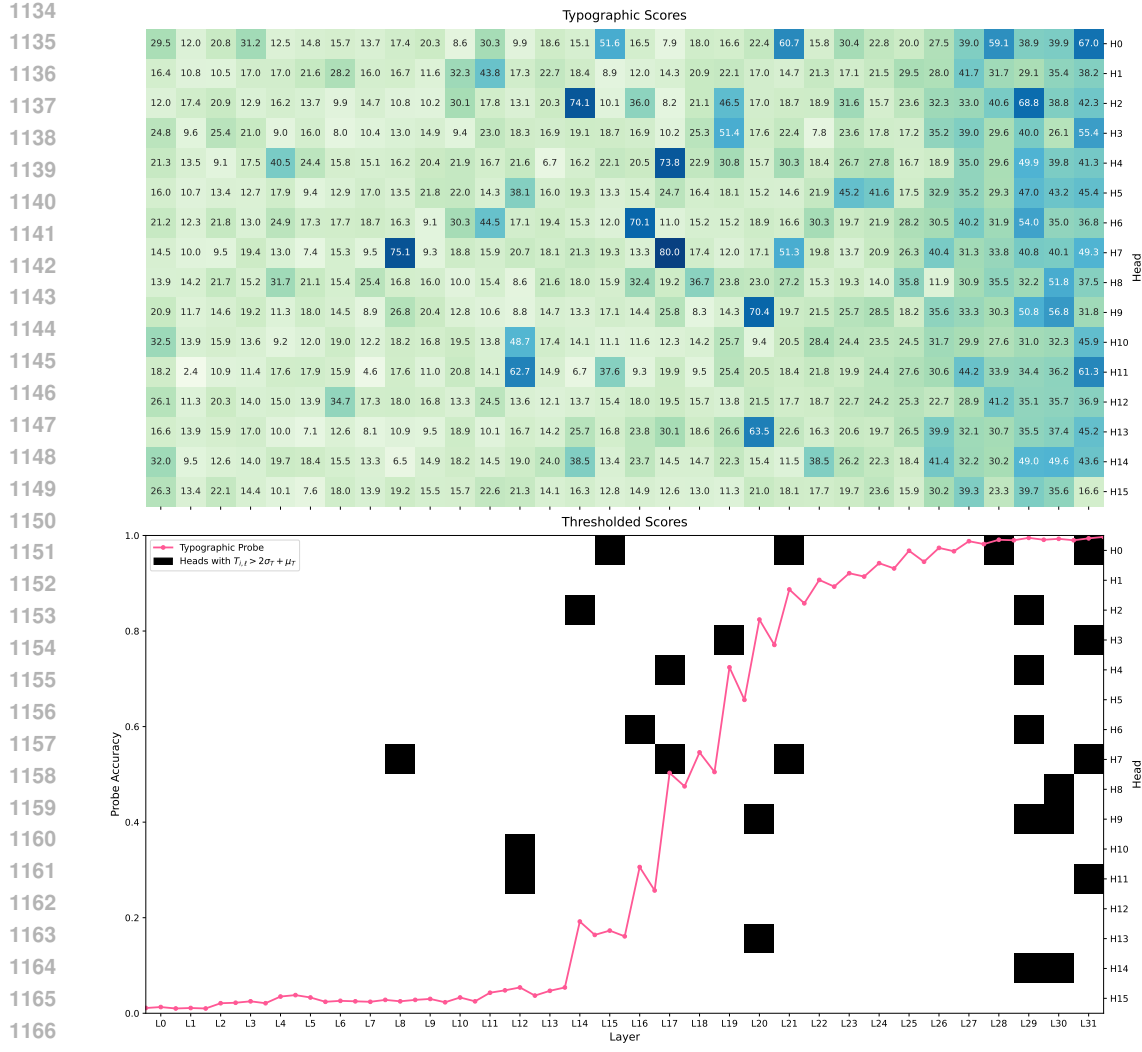


Figure 13: ViT-H typographic attention scores  $T_{i,\ell}$  (top), thresholded and compared with linear probe accuracies (bottom). Layers with higher typographic attention scores align with increased probe accuracy, highlighting a correspondence between attention patterns and typographic feature decodability.

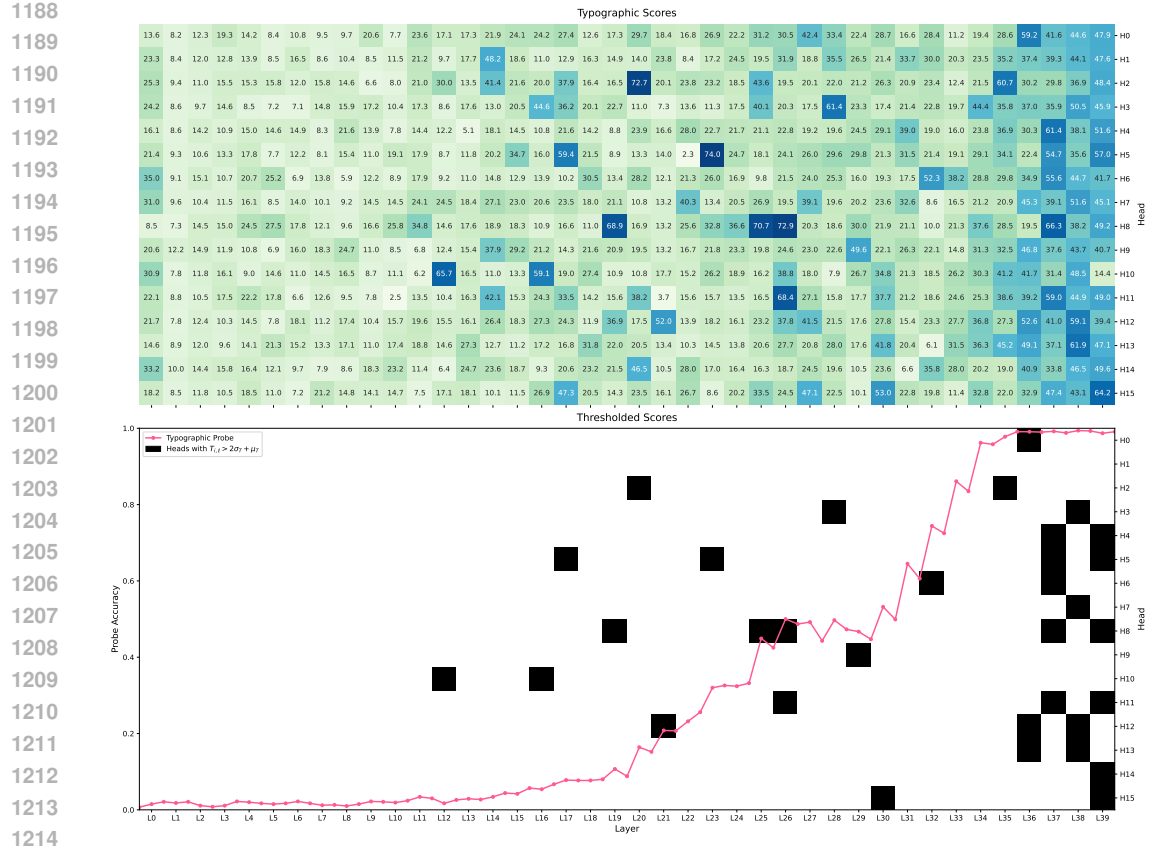


Figure 14: ViT-G typographic attention scores  $T_{i,\ell}$  (top), thresholded and compared with linear probe accuracies (bottom). Layers with higher typographic attention scores align with increased probe accuracy, highlighting a correspondence between attention patterns and typographic feature decodability.

1215  
1216  
1217  
1218  
1219  
1220  
1221  
1222  
1223  
1224  
1225  
1226  
1227  
1228  
1229  
1230  
1231  
1232  
1233  
1234  
1235  
1236  
1237  
1238  
1239  
1240  
1241

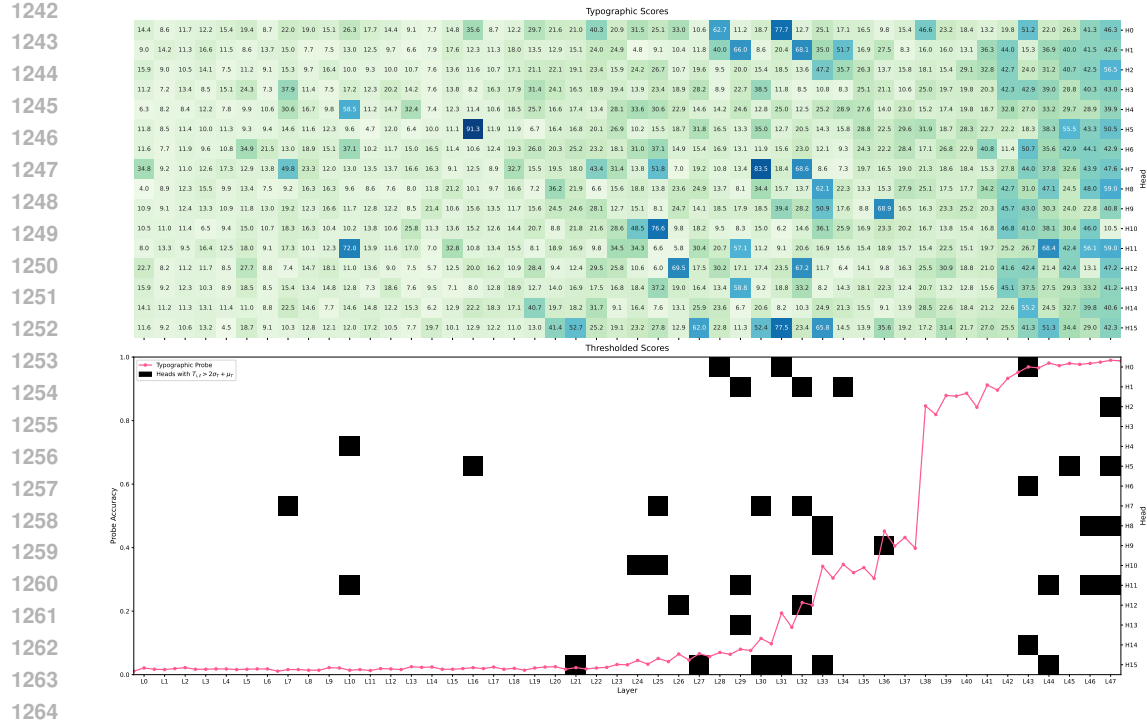


Figure 15: VII-BigG typographic attention scores  $T_{i,l}$  (top), thresholded and compared with linear probe accuracies (bottom). Layers with higher typographic attention scores align with increased probe accuracy, highlighting a correspondence between attention patterns and typographic feature decodability.